Physical and Optical Properties of Aged Biomass Burning Aerosol from Wildfires in Siberia and the Western US at the Mt. Bachelor Observatory

5   James R. Laing[1], Dan A. Jaffe[1,2], Jonathan R. Hee[1]

[1] University of Washington-Bothell, Bothell, WA, USA
[2] University of Washington, Seattle, WA, USA
Correspondence to: Dan A. Jaffe (djaffe@uw.edu)

10   **Abstract.** The summer of 2015 was an extreme forest fire year in the Pacific North West. Our sample site at Mt. Bachelor Observatory (MBO, 2.7 km a.s.l.) in central Oregon observed biomass burning events more than 50% of the time during August. In this paper we characterize the aerosol physical and optical properties of 19 aged biomass burning (BB) events during August 2015. Six of the nineteen events were influenced by Siberian fires originating near Lake

15   Baikal. The remainder of the events resulted from wildfires in Northern California and Southwestern Oregon with transport times to MBO ranging from 4.5-35 hours. Fine particulate matter (PM1), carbon monoxide (CO), aerosol light scattering (σ_{scat}) and absorption (σ_{abs}), and aerosol number size distributions were measured throughout the campaign. We found that the Siberian events had significantly higher $\Delta\sigma_{abs}/\Delta CO$ enhancement ratio, higher mass absorption

20   efficiency (MAE; $\Delta\sigma_{abs}/\Delta PM1$), lower single scattering albedo (ω), and lower Absorption Ångström exponent (AAE) when compared with the regional events. We suspect the Siberian events observed represent a portion of the fire plume that has hotter flaming fire conditions that enabled strong pyro-convective lofting and long transport to MBO. These plumes would then have preferentially higher black carbon emissions and thus absorption enhancement. The lower

25   AAE values in the Siberian events compared to regional events indicates a lack of brown carbon (BrC) production by the Siberian fires or a loss of BrC during transport. We found that mass scattering efficiencies (MSE) for the BB events to range from 2.50-4.76 m^2 g^{-1}. We measured aerosol size distributions with a scanning mobility particle sizer (SMPS). Number size distributions ranged from unimodal to bimodal and had geometric mean diameters ranging from

30   138-229 nm and geometric standard deviations ranging from 1.53-1.89. We found MSE's for BB events to be positively correlated with the geometric mean of the aerosol size distributions ($R^2 =$

0.73), which agrees with Mie Theory. We did not find any dependence on event size distribution to transport time or fire source location.

1. Introduction

35   Biomass burning (BB) is a major source of aerosol in the atmosphere [*Andreae and Merlet*, 2001; *Bond et al.*, 2004]. BB particles are predominantly organic carbon (OC) and black carbon (BC), with some inorganic material [*Reid et al.*, 2005b; *Vakkari et al.*, 2014]. These particles can significantly impact the Earth's radiative balance and climate through direct and indirect aerosol effects. The direct effects on radiative forcing are due to the light scattering and

40   absorption of the aerosol [*Boucher et al.*, 2013; *Haywood and Boucher*, 2000], and the indirect effects are caused by particles acting as cloud condensation nuclei (CCN) which affects cloud albedo [*Pierce et al.*, 2007; *Spracklen et al.*, 2011]. According to the IPCC 2013 report the largest uncertainty in determining global radiative forcing comes from quantifying the direct and indirect effects of aerosols [*Boucher et al.*, 2013]. Biomass burning is a major contributor to

45   global aerosol burden and it has been predicted that these emissions are likely to increase due to climate change, particularly in the boreal forests of North America and Russia [*Flannigan et al.*, 2009; *Stocks et al.*, 1998] and the western U.S. [*Y Liu et al.*, 2014b; *Westerling et al.*, 2006]. This makes the proper characterization of aged BB emissions even more important.

        Currently there are few field measurements of well-aged BB emissions. Our knowledge

50   of BB aerosol primarily comes from laboratory experiments and near-field measurements taken within a few hours of a wildfire [*May et al.*, 2015; *May et al.*, 2014; *Okoshi et al.*, 2014; *Vakkari et al.*, 2014; *Yokelson et al.*, 2013b; *Yokelson et al.*, 2009]. *Holder et al.* [2016] showed that laboratory measurements of aerosol optical properties do not accurately reproduce field measurements. Freshly emitted BB particles are small in diameter (30-100 nm) [*Hosseini et al.*,

55   2010; *Levin et al.*, 2010]. As the plume ages, the aerosol undergo rapid chemical and physical changes on the time scale of minutes to hours [*Reid et al.*, 2005a; *Reid et al.*, 2005b; *Vakkari et al.*, 2014]. The change in particle size is due to coagulation and the condensation of organic material onto the existing particles [*Reid et al.*, 2005b; *Seinfeld and Pandis*, 2006]. The coagulation rate can be very high in fresh BB plumes since this is equivalent to the square of

60   particle number concentration. This process increases the size of the particles while decreasing

the number concentration. Condensation of secondary organic aerosol (SOA) onto particles in BB plumes can also increases particle size. The condensation of SOA is counterbalanced by the loss of primary organic aerosol (POA), which can evaporate during plume dilution [*May et al.*, 2015; *May et al.*, 2013]. The net condensation/evaporation effect is highly variable. Some studies

65 have observed an increase in mass with plume age due to SOA production [*Briggs et al.*, In Press; *Hobbs*, 2003; *Vakkari et al.*, 2014; *Yokelson et al.*, 2009], while others have observed limited SOA formation [*Akagi et al.*, 2012; *Jolleys et al.*, 2015]. All of these uncertainties in the aging process of biomass burning underscores the importance of characterizing the physical and optical properties of well-aged biomass burning aerosol.

70   In this study we analyze the physical and optical aerosol properties of 19 aged BB events observed in the summer of 2015 at Mt. Bachelor in Oregon. The BB events consisted of Regional events (fires in Northern California and Southwestern Oregon; transported 3-30 hours) and Siberian fire events (fires around Lake Baikal; transported 4-10 days). We investigated the aerosol optical and physical properties of these events and explored their variation with source

75 location and transport time. This study addresses the following questions:

- What are the differences in the optical properties of regional and Siberian BB events observed at MBO?
- What is the range of mass scattering efficiencies for BB events and what explains their variability?

80 - What is the range in aerosol size distributions of BB events at MBO and how does this vary with plume age?

2. Methods

2.1. Mt Bachelor Observatory

The Mt. Bachelor Observatory (MBO) is a mountaintop site that has been in operation since

85 2004 [*Jaffe et al.*, 2005] . It is located at the summit of Mt. Bachelor in central Oregon, US (43.98° N, 121.69° W, 2,764 m a.s.l.). A suite of measurements (including carbon monoxide (CO), ozone (O_3), aerosol scattering, and more) have been made continuously at the summit site since 2004. Previous studies have observed BB plumes in the free troposphere from regional and distant sources in the spring, summer, and fall [*Baylon et al.*, 2015; *Briggs et al.*, In Press;

90   *Collier et al.*, Submitted; *Timonen et al.*, 2014; *Weiss-Penzias et al.*, 2007; *Wigder et al.*, 2013],
      and long-range transport of Asian pollution in the spring [*Ambrose et al.*, 2011; *Fischer et al.*,
      2010a; *Fischer et al.*, 2010b; *Gratz et al.*, 2014; *Jaffe et al.*, 2005; *Reidmiller et al.*, 2010;
      Timonen et al., 2014; *Timonen et al.*, 2013; *Weiss-Penzias et al.*, 2006]. During the summer of
      2015 an intensive field campaign was performed at MBO to measure aerosol physical and optical
95   properties of wildfire emissions.

2.2. CO, CO₂, and meteorological data

CO and CO_2 measurements were made using a Picarro G2302 Cavity Ring-Down Spectrometer.
Calibrations were performed every 8 hours using three different NOAA calibration gas
standards, which are referenced to the World Meteorological Organization's (WMO) mole
100   fraction calibration scale [*Gratz et al.*, 2014]. Basic meteorology measurements, such as
      temperature, humidity and wind speed are also measured continuously [*Ambrose et al.*, 2011].

2.3. Aerosol Instruments

We measured dry (relative humidity (RH) less than 35%) aerosol scattering and absorption
coefficients, aerosol number size distribution, and particle mass during the 2015 summer
105   campaign in 5 minute averages. The aerosol instruments were located in a temperature-
      controlled room within the summit building, situated approximately 15 m below the inlet. A 1
      µm impactor was located inline prior to any The aerosol sample line was situated such that the
      last 2.5 m was located within a space that was temperature controlled at $20 \pm 3°C$, typically
      10°C–20°C warmer than ambient. Relative humidity of the sampled air was less than 35%
110   throughout the campaign. The temperature increase from outside into the heated building
      reduced the RH of the sample. RH was measured in the sample airstream by the nephelometer
      and SMPS. The average RH during the campaign measured by the nephelometer and SMPS was
      22.1% and 22.6%, respectively. Ninety- five percent of the 5 minute averaged samples had an
      RH less than 30%.
115   We measured multiwavelength aerosol light scattering (σ_{scat}) using an integrating
      nephelometer (model 3563, TSI Inc., Shoreview, MN) at wavelengths 450, 550, and 700 nm.
      Anderson and Ogren (1998) corrections were applied to the σ_{scat} coefficients [*Fischer et al.*,
      2010a]. We measured aerosol light absorption (σ_{abs}) with a 3λ tricolor absorption photometer

(TAP, Brechtel Inc., Hayward, CA) at wavelengths 467, 528, and 660 nm. Throughout the paper

120 σ_{scat} and σ_{abs} values represent measurements taken at 550 nm and 528 nm, respectively. The TAP

is a new instrument that uses the same operating principle as the Particle Soot Absorption

Photometer (PSAP) and the same filters (47 mm PALL E70-2075W). Unlike the PSAP, the TAP

rotates through 8 filter spots per individual filter along with two reference spots. During

deployment at MBO, the TAP was set to rotate to the next filter spot when filter spot's

125 transmission reached 50%. The absorption coefficients were corrected using the filter loading

and aerosol scattering correction factors derived for the 3λ PSAP by *Virkkula* [2010].

Single scattering albedo (ω) for each event was calculated as the RMA regression of

scattering and total extinction (scattering + absorption) coefficient at 528 nm. To adjust the σ_{scat}

value from 550 nm-528 nm, a power law relationship was assumed between scattering and

130 wavelength. The 450-550 nm pair was used to adjust the 550 nm σ_{scat} measurement to 528 nm

using the equation: $\sigma_{scat}^{528} = \sigma_{scat}^{550} * \left(\frac{\lambda_{550}}{\lambda_{528}}\right)^{SAE_{450,550}}$, where λ is wavelength and SAE is the

scattering Ångström exponent calculated with the two wavelengths specified. Absorption

Ångström exponent (AAE) values were calculated for the absorption coefficient pair of 467 and

660 nm [*Fischer et al.*, 2010a].

135 We measured 5 minute averaged dry aerosol number size distribution with TSI 3938

Scanning Mobility Particle Sizer (SMPS). The SMPS system consisted of a TSI 3082

electrostatic classifier with TSI 3081 Differential Mobility Analyzer (DMA) and TSI 3787

water-based condensation particle counter. A total of 107 bins were used to measure a diameter

range from 14.1-637.8 nm. A sheath to aerosol flow ratio of 10:1 was used for the DMA. A

140 multiple charge correction and diffusion loss correction were applied to the SMPS particle

number concentration data using the TSI software. An additional diffusion correction for the

inlet tube (15 m, 12 LPM) was applied assuming a laminar flow [*Hinds*, 1999]. Prior to

deployment we confirmed the sizing accuracy of the SMPS using polystyrene latex spheres

(PSL).

145 We measured dry particle mass under 1 μm (PM1) with an Optical Particle Counter

(OPC, model 1.109, Grimm Technologies, Douglasville, GA). This is a U.S. EPA equivalent

method for measuring PM2.5 mass concentration. The OPC was factory calibrated prior to

deployment.

All particle measurements (σ_{scat}, σ_{abs}, PM1, number size distribution) were corrected to

150   standard temperature and pressure (STP; T = 273.15, P = 101.325 kPa).

2.4. Enhancement ratio calculations

Enhancement ratios ($\Delta Y/\Delta X$) were calculated from the slope of the RMA regression of Y plotted

against X. *Briggs et al.* [In Press] calculated enhancement ratios (ERs) of BB plumes using three

different methods, one being the RMA slope of the linear correlation of two species, and two

155   calculating absolute enhancement above local background using two different definitions of

background. All three methods produced similar results for $\Delta\sigma_{scat}/\Delta CO$, $\Delta NO_y/\Delta CO$, and

$PAN/\Delta CO$, but differing results for $\Delta O_3/\Delta CO$. In our study we will use the RMA regression

method for calculating ERs of $\Delta\sigma_{scat}/\Delta CO$ and $\Delta\sigma_{abs}/\Delta CO$.

Mass scattering and mass absorption efficiencies (MSE and MAE) were calculated as the

160   enhancement ratios of $\Delta\sigma_{scat}/\Delta PM1$ and $\Delta\sigma_{abs}/\Delta PM1$, respectively, at 550 nm for σ_{scat} and 528

nm for σ_{abs}. In all cases the enhancements (Δ) are large compared to background, thus avoiding

the problems described by *Briggs et al.* [In Press] for small enhancements above background.

2.5. Biomass burning event identification

We identified BB events as time periods during which 5-min ambient aerosol scattering $\sigma_{scat} > 20$

165   Mm^{-1} for at least one hour, 5-min CO > 150 ppbv for at least one hour, and a strong correlation

($R^2 > 0.80$) was found between σ_{scat} and CO. To determine fire locations we calculated back-

trajectories using the National Oceanic and Atmospheric Administration Hybrid Single-Particle

Lagrangian Integrated Trajectory (HYSPLIT) model, version 4 [*Draxler*, 1999; *Draxler and

Hess*, 1997; 1998; *Stein et al.*, 2015]. We used the Global Data Assimilation System (GDAS) 1°

170   × 1° gridded meteorological data from the National Oceanographic and Atmospheric

Administration's Air Resources Laboratory (NOAA-ARL). Within GDAS, the grid containing

MBO is located at ~1500 m amgl (above model ground level) so back-trajectory starting heights

of 1300, 1500, and 1700 m amgl were chosen [*Ambrose et al.*, 2011]. We identified fire locations

using Moderate Resolution Imaging Spectroradiometer (MODIS) satellite-derived active fire

175   counts [*Justice et al.*, 2002]. Similar criteria for identifying BB events has been used by *Baylon

et al.* [2015] and *Wigder et al.* [2013] from data collected at MBO.

3. Results and Discussion

3.1. Identified BB events and Fire Source Identification

The summer of 2015 was a very active fire season in the Pacific North West (Figure 1). During
the month of August 2015, 51% of the 5 minute averages met the criteria for a BB event of
having $\sigma_{scat} > 20$ Mm^{-1} and CO > 150 ppbv, including several multi-day periods. We split these
multi-day events up if discernable plumes within the event could be identified. Altogether we
identified 19 events, ranging from 1.5-45 hours in duration. We use the term event, not plume,
because of the long duration of some of the events and the fact that most BB events observed in
2015 were influenced by emissions from multiple fires.

We categorized most of the events into three main periods (Figure 2). Periods 1 (8/9/15-
8/12/15: events 2-8) and 3 (8/23/15-8/29/15: events 16-19) are both multi-day periods that
experienced regional BB smoke from fires in Northern California and Southwestern Oregon.
Transport time from these regional fires to MBO, estimated from the back-trajectories, ranged
from 3-30 hours. Period 3 (8/17/15-8/22/15: events 10-15) is characterized by influence from
Siberian BB events. During August there were intense forest fires around Lake Baikal in Siberia,
peaking on 8/8/2015 with a total fire area of 681 km^2, and an estimated CO and BC emissions of
$3.22\text{x}10^8$ and $1.33\text{x}10^6$ kg/day, respectively (*Fire INventory from NCAR (FINN) data)
[Wiedinmyer et al., 2011]*. Transport times from the Northeastern Asia to MBO during these
events ranged from 4-10 days. NASA MODIS aqua and terra images show the eastward
transport of smoke from the Lake Baikal fires during this time period
[*https://worldview.earthdata.nasa.gov/*, 2016]. We used V3.30 aerosol classification products
from the Cloud-Aerosol Lidar with Orthogonal Polarization (CALIOP) instrument on the Cloud-
Aerosol Lidar Infrared Pathfinder Satellite Observation (CALIPSO) satellite to confirm the
transport of plumes of smoke from the Siberian fires to North America [*http://www-
calipso.larc.nasa.gov/*, 2016; *Winker et al.*, 2010; *Winker et al.*, 2009]. Aerosol plumes are
identified as one of six types: dust, polluted continental, polluted dust, smoke (biomass burning),
clean continental or clean marine aerosols [*Omar et al.*, 2009].

3.2. Overview of Summer 2015 BB Events from difference sources

205 Table 1 provides an overview of the 19 BB events from MBO during the summer of 2015. We
calculated water vapor enhancement (ΔWV) to indicate the origin of the event air mass. Positive
ΔWV suggest the air mass ascended from the boundary layer (BL) to while near zero or
negative values mean the air mass is relatively dry and likely descended or arrived from the free
troposphere (FT) [*Baylon et al.*, 2015; *Wigder et al.*, 2013]. All of the regional BB events have

210 ΔWV values ≥ 1.00, while all of the Siberian influenced events have ΔWV values near zero or
negative.

We found the $\Delta\sigma_{scat}/\Delta CO$ (σ_{scat} at STP) enhancement ratio to range from 0.48-1.29 Mm^{-1}/ppbv, with the majority of events being between 0.8 and 1.25 Mm^{-1}/ppbv. We found
$\Delta PM1/\Delta CO$ (PM1 at STP) to range from 0.18-0.43 µg cm^{-3}/ppbv. These values are in the same

215 range as BB plumes seen previously at MBO [*Baylon et al.*, 2015; *Wigder et al.*, 2013].

3.3. Optical Properties of the BB Aerosol at MBO

We observed significant differences in the optical properties of regional and Siberian influenced
BB events. The Siberian influenced events had enhanced absorption coefficients relative to other
measurements made. This resulted in higher $\Delta\sigma_{abs}/\Delta CO$, higher MAE, and lower ω ($\sigma_{scat}/(\sigma_{scat} +$

220 $\sigma_{abs})$) compared to regional BB events (Figure 3 and 4). We found no significant differences for
$\Delta\sigma_{scat}/\Delta CO$ or MSE between regional and Siberian events. Event 9 was anomalous in that it has
very low absorption enhancement, a high ω, and is not part of the designated Periods defined in
section 3.1. Back-trajectories show that event 9 came from the boundary layer under stagnant
conditions, indicating an aged and mixed source. Back-trajectories for the Siberian events

225 (events 10-15) indicate that the plumes were lofted to altitudes of 4-10 km (Figure S1). The
Siberian events at MBO were observed over the course of a week (8/17/2015-8/23/2015),
therefor the back-trajectories in Fig. S1 represent a sustained meteorological pattern that
consistently transported Siberian smoke to North America throughout the week. Aerosol vertical
profiles measured by CALIOP corroborate the transport of BB plumes from the Siberian fires

230 across the Pacific at altitudes of 4-10 km. Large BB plumes were identified over Northeast Asian
and the North Pacific consisting primarily of BB smoke and some polluted dust over the
Northern Pacific from 8/8/2015-8/17/2015. Figures S2-S5 show selected CALIPSO transects
from 8/13/2015-8/16/2015 over the Pacific. The location and altitude of these plumes match the

back-trajectories calculated from MBO for the Siberian events (Figure S1), verifying that events

235 10-15 are heavily influenced by the Siberian fires.

We theorize the Siberian BB events observed at MBO represent hotter, more flaming fires which have higher BC emissions and thus higher absorption enhancements compared to the regional BB events. During the ARCTAS-A flight campaign in Alaska, Siberian fire plumes were found to have a much larger BC/CO ratio (8.5 ± 5.4 ng m-3/ppbv) than North American

240 fire plumes (2.3 ± 2.2 ng m-3/ppbv) [*Kondo et al.*, 2011]. This difference was attributed to the Siberian fires having a higher modified combustion efficiency (MCE). In addition, for the Siberian BB plumes they found MCE to increase with altitude. *Jolleys et al.* [2015] correspondingly found higher ΔBC/ΔOA ratios to increase with altitude in Eastern Canadian BB plumes. Intense, flaming fire plumes have higher injection heights into the atmosphere due to

245 enhanced pyro-convection, whereas smoldering fires have low thermal convective energy and are mostly contained within the boundary layer. BB aerosol lofted to the free troposphere via pyro-convection is less likely to be removed and can have a longer atmospheric lifetime of up to 40 days [*Bond et al.*, 2013]. The back-trajectories for the Siberian events corroborate this idea. They were all relatively dry (water vapor mixing ratio < 5 g kg^{-1}) with little precipitation during

250 transport, suggesting the aerosol in the Siberian events was subjected to very limited wet deposition, which is the main removal mechanism from the atmosphere. Flaming conditions produce more black carbon (BC) and less organic aerosol (OA) generally, which leads to amplified absorption [*Vakkari et al.*, 2014; *Yokelson et al.*, 2009]. Flaming conditions are associated with high modified combustion efficiency (MCE) values [*Reid et al.*, 2005a].

255 Unfortunately we were not able to calculate MCE values for the Siberian events at MBO due to extensive dilution and boundary layer mixing during transport [*Yokelson et al.*, 2013a].

We found AAE values for the Siberian events to be significantly lower than regional BB events (Figures 3 and 4). High AAE values are indicative of the presence of brown carbon (BrC). Brown carbon is a fraction of organic aerosol (OA) that selectively absorbs short wavelengths

260 [*Andreae and Gelencser*, 2006; *Chen and Bond*, 2010; *Kirchstetter et al.*, 2004]. There are two possible explanations for the difference in AAE values. The first is that the flaming conditions that produced the Siberian events seen at MBO had higher BC and lower OA emissions, which inherently have lower AAE as total absorption is dominated by BC and there is less BrC in the aerosol. Laboratory and field studies have corroborated this and observed an inverse relationship

265 between MCE and AAE [*Holder et al.*, 2016; *S Liu et al.*, 2014a; *McMeeking et al.*, 2014]. The other explanation is that BrC is lost during transport through photobleaching, volatilization, and aerosol-phase reactions. *Forrister et al.* [2015] determined that BrC decreased with transport with a half-life of 9 hours and that AAE decreases from ~4.0 to ~2.5 24 hours after emission. All of the regional BB events (Periods 1 and 3) were influenced by multiple fires that had transport

270 times varying from 3- 30 hours. With each event being influenced by at least one fire with a transport time ≤ 6 hours, this short transport time is consistent with the higher AAE values we observed.

3.4. Mass Scattering Efficiency

Mass scattering efficiencies (MSE) are important for calculating the radiative forcing effects of

275 aerosols in global climate and chemical transport models. Estimates of MSE are used to convert aerosol mass measurements to aerosol optical properties [*Briggs et al.*, In Press; *Hand and Malm*, 2007; *Pitchford et al.*, 2007]. MSE is dependent on particle composition, which determines the particle's refractive index and hygroscopy, and aerosol size distribution [*Hand and Malm*, 2007]. We calculated MSE's as the slope of the RMA regression of σ_{scat} and PM1

280 ($\Delta\sigma_{scat}/\Delta$PM1). R^2 values were >0.94 for all events. We found MSE values to range from 2.50-4.76 $m^2\ g^{-1}$, which are consistent with previously measured values.

During 2013 at MBO, MSE values estimated using AMS organic matter (OM) data and the σ_{scat} for four wildfire plumes ranged from 2.8-4.8 $m^2\ g^{-1}$ (mean: 3.7 $m^2\ g^{-1}$) [*Briggs et al.*, In Press]. *Levin et al.* [2010] calculated MSE values for fresh BB smoke from a variety of fuels to

285 range from 1.5–5.7 $m^2\ g^{-1}$, with most of the values falling between 2.0 and 4.5 $m^2\ g^{-1}$. *Reid et al.* [2005a] reviewed MSE values from BB events and found a range between 3.2 and 4.2 $m^2\ g^{-1}$ (mean: 3.8 $m^2\ g^{-1}$) for temperate and boreal fresh smoke, and larger values for aged smoke (3.5-4.6 $m^2\ g^{-1}$; mean: 4.3 $m^2\ g^{-1}$). MSE values upwards of ~6 $m^2\ g^{-1}$ have been observed for aged BB [*Hand and Malm*, 2007; *McMeeking et al.*, 2005]. Due to the large variation in MSE values for

290 BB events, assigning an average MSE value to convert aerosol mass measurements to aerosol optical properties or vice versa introduces significant uncertainties.

We investigated the cause for variation in the MSE values we observed (Figure 5). We found MSE's for BB events to be positively correlated with D_{pm} ($R^2 = 0.73$) (Figure 5a). If two D_{pm} values associated with bimodal size distributions are removed the correlation increases

295   substantially ($R^2 = 0.88$). A positive correlation between MSE and mean particle diameter has previously been observed in ambient data [*Lowenthal and Kumar*, 2004] and laboratory studies [*McMeeking et al.*, 2005]. Theoretically according to Mei theory, MSE will increases as the average particle diameter grows, through coagulation and condensation, toward the measurement wavelength (550 nm) [*Seinfeld and Pandis*, 2006].

300   MSE was also well correlated with event integrated σ_{scat} and PM1 mass, and slightly correlated with CO (Figure 5b,c,d). The dependence of MSE on mass concentration [*Malm and Hand*, 2007] and σ_{scat} [*Lowenthal and Kumar*, 2004] has previously been observed, although it is mainly thought to be a function of particle size.

3.5. BB Size Distributions

305   Figure 6 shows the BB aerosol number size distributions for the events we observed at MBO in dN/dlogDp (Figure 6). We found D_{pm} and σ_g of the number distributions to range from 138-229 nm and 1.53-1.89, respectively. The size distributions observed at MBO are similar to *Janhäll et al.* [2010], who compiled aged biomass burning size distributions. They found the accumulation mode mean diameter to range from 175- 300 nm with geometric standard deviations of 1.3–1.7.

310   During the ARCTAS-B flight campaign, aged BB plumes of Western Canadian and Asian origins were found to have similar size distributions (Canadian: $D_{pm} = 224 \pm 14$ nm, $\sigma_g = 1.31 \pm 0.05$; Asian: $D_{pm} = 238 \pm 11$ nm, $\sigma_g = 1.31 \pm 0.03$) [*Kondo et al.*, 2011]. The BORTAS-B flight campaign in Eastern Canada observed aged BB plumes with median diameters of 180-240 nm [*Sakamoto et al.*, 2015].

315   We observed clear bimodal distributions with an accumulation mode (100-500 nm) and Aitken mode (20-100 nm) for five events (2, 3, 11, 14 and 15). The Aitken mode in these size distributions most likely represents a secondary source from within the boundary layer. A prominent "tail" consisting of higher than expected number concentrations of small-diameter particles (30-90 nm) was observed for most of the unimodal events at MBO. It would be

320   expected that particles in this size range would grow to larger particles through coagulation relatively quickly. *Sakamoto et al.* [2015] observed a similar elevation in the number concentration of small particles during the BORTAS-B campaign. They attempted to account for the existence of the tail with a Lagrangian box model of coagulation and dilution but were unable to do so. Coagulation should cause a significant decrease in Aitken mode particles in a matter of

325   hours; and nucleation and condensation growth rates would have to be unreasonably high to maintain these small particles.

We observed no clear distinction between the size distributions from regional and Siberian events. These results are consistent with previous studies that have not observed a dependence from plume age, transport time, or source location on the BB size distribution.

330   *Kondo et al.* [2011] found little difference between the D_{pm} of Siberian and Canadian BB plumes despite different chemical composition and optical properties, and transport times. Similarly, *Sakamoto et al.* [2015] found no trend in size distribution with plume transport distance. We found event integrated D_{pm} to be correlated with event integrated σ_{scat} ($R^2 = 0.65$) and PM1 mass ($R^2 = 0.72$), and moderately correlated with CO ($R^2 = 0.40$). D_{pm} was not found to be

335   correlated with any normalized enhancement ratio ($\Delta\sigma_{scat}/\Delta CO$, $\Delta PM1/\Delta CO$). Therefore, the more concentrated the BB plume, the larger the size distribution.

In a related study, *Sakamoto et al.* [In Press], we selected subsets of the MBO BB regional events presented here and tested them against parameterizations of the aged size distribution. The parameterizations calculate D_{pm} and σ_g from inputs that can be derived from

340   emissions-inventory and meteorological parameters. The seven inputs are: emission median dry diameter, emission distribution modal width, mass emissions flux, fire area, mean boundary-layer wind speed, plume mixing depth, and time/distance since emission. We identified eleven plumes from regional events that had consistent transport to known regional fires. The simple fits captured over half of the variability in observed D_{pm} and modal width, even though the freshly

345   emitted D_{pm} and modal widths were unknown. The results demonstrate that the parameterizations presented in *Sakamoto et al.* [In Press] section 3.4 can be successfully used to estimate aged BB size distributions in regional BB plumes with transport times up to 35 hours. Using these parameterizations to estimate BB plume size distribution in global and regional aerosol models is a significant improvement to assuming fixed values for size-distribution parameters.

350   **4. Conclusions**

We characterized the physical and optical properties of 19 aged biomass burning events observed at the Mt. Bachelor Observatory in the summer of 2015. Regional (Northern California and Southwestern Oregon) and Siberian events were observed. Our main conclusions were:

- $\Delta\sigma_{scat}/\Delta CO$ (σ_{scat} at STP) enhancement ratio to range from 0.48-1.29 Mm^{-1}/ppbv, with

355   the majority of events being between 0.8 and 1.25 Mm^{-1}/ppbv.

- Siberian influenced events had significantly higher $\Delta\sigma_{abs}/\Delta CO$ and MAE, and lower ω compared to regional events. We propose this is due to MBO sampling the portion on Siberian smoke that has been lofted to higher elevation through pyro-convection., thereby preferentially sampling emissions of strong flaming combustion conditions. In general

360   flaming conditions produce more BC, which would explain the amplified absorption in the Siberian events.

- Absorption Ångström exponent values were significantly lower for the Siberian events than regional events, which indicates lack of BrC produced by the Siberian fires or loss of BrC during transport through photobleaching, volatilization, and aerosol-phase reactions.

365 - Mass scattering efficiencies ranged from 2.50-4.76 m^2 g^{-1}. MSE was positively correlated with D_{pm} ($R^2 = 0.73$), which agrees with Mie theory.

- Aerosol number size distribution D_{pm} and σ_g ranged from 138-229 nm and 1.53-1.89, respectively. Five of the nineteen events had bimodal distributions, the rest being unimodal. The unimodal distributions had a prominent "tail" of small-diameter particles

370   (30-90 nm). No distinction could be made between regional and Siberian size distributions.

5. Author Contribution

J.R. Laing preformed the data analysis and prepared the manuscript with assistance from all co-authors.

6. Acknowledgments

Funding for research at MBO was supported by the National Science Foundation (grant number: 1447832). The MBO is also supported by a grant from the NOAA Earth System Research Laboratory. The views, opinions and findings contained in this report are those of the author(s) and should not be construed as an official National Oceanic and Atmospheric Administration or U.S. Government position, policy or decision. The authors gratefully acknowledge the NOAA Air Resources Laboratory (ARL) for the provision of the HYSPLIT

transport model used in this publication. The CALIPSO satellite products was supplied from the NASA Langley Research Center.

385

References:

Akagi, S. K., et al. (2012), Evolution of trace gases and particles emitted by a chaparral fire in California, *Atmospheric Chemistry and Physics*, *12*, 1397-1421, doi:10.5194/acp-12-1397-2012.

Ambrose, J. L., D. R. Reidmiller, and D. A. Jaffe (2011), Causes of high O(3) in the lower free troposphere over the Pacific Northwest as observed at the Mt. Bachelor Observatory, *Atmospheric Environment*, *45*, 5302-5315, doi:10.1016/j.atmosenv.2011.06.056.

Andreae, M. O., and A. Gelencser (2006), Black carbon or brown carbon? The nature of light-absorbing carbonaceous aerosols, *Atmospheric Chemistry and Physics*, *6*, 3131-3148.

Andreae, M. O., and P. Merlet (2001), Emission of trace gases and aerosols from biomass burning, *Global Biogeochemical Cycles*, *15*, 955-966, doi:10.1029/2000gb001382.

Baylon, P., D. A. Jaffe, N. L. Wigder, H. Gao, and J. Hee (2015), Ozone enhancement in western US wildfire plumes at the Mt. Bachelor Observatory: The role of NOx, *Atmospheric Environment*, *109*, 297-304, doi:http://dx.doi.org/10.1016/j.atmosenv.2014.09.013.

Bond, T. C., et al. (2013), Bounding the role of black carbon in the climate system: A scientific assessment, *J. Geophys. Res.*, *118*, 1-173, doi:10.1002/jgrd.50171.

Bond, T. C., D. G. Streets, K. F. Yarber, S. M. Nelson, J. H. Woo, and Z. Klimont (2004), A technology-based global inventory of black and organic carbon emissions from combustion, *Journal of Geophysical Research-Atmospheres*, *109*(D14), 43, doi:10.1029/2003jd003697.

Boucher, O., et al. (2013), Clouds and Aerosols, in *Climate Change 2013: The Physical Science Basis. Contribution of Working Group I to the Fifth Assessment Report of the Intergovernmental Panel on Climate Change*, edited by T. F. Stocker, D. Qin, G.-K. Plattner, M. Tignor, S. K. Allen, J. Boschung, A. Nauels, Y. Xia, V. Bex and P. M. Midgley, Cambridge University Press, Cambridge, UK.

Briggs, N. L., D. A. Jaffe, H. Gao, J. Hee, P. Baylon, Q. Zhang, S. Zho, S. Collier, P. D. Sampson, and R. A. Cary (In Press), Particulate matter, ozone, and nitrogen species in aged wildfire plumes observed at the Mount Bachelor Observatory, a high elevation site in the Pacific Northwest, *Aerosol and Air Quality Research*.

Chen, Y., and T. C. Bond (2010), Light absorption by organic carbon from wood combustion, *Atmospheric Chemistry and Physics*, *10*(4), 1773-1787.

Collier, S., et al. (Submitted), Regional Influence of Aerosol Emissions from Wildfires Is Governed by Combustion Efficiency: Insights from the BBOP Campaign, *Environmental Science and Technolgy*, *submitted*.

Draxler, R. R. (1999), HYSPLIT4 user's guide, NOAA Tech. Memo*Rep.*, NOAA Air Resources Laboratory, Silver Spring, MD.

Draxler, R. R., and G. D. Hess (1997), Description of the HYSPLIT_4 modeling system, NOAA Tech. Memo*Rep.*, 24 pp, NOAA Air Resources Laboratory, Silver Spring, MD.

Draxler, R. R., and G. D. Hess (1998), An overview of the HYSPLIT_4 modeling system of trajectories, dispersion, and deposition, *Australian Meteorological Magazine*, *47*, 295-308.

Fischer, E. V., D. A. Jaffe, N. A. Marley, J. S. Gaffney, and A. Marchany-Rivera (2010a),
Optical properties of aged Asian aerosols observed over the US Pacific Northwest, *Journal of
Geophysical Research-Atmosphers*, *115*, D20209-D20209, doi:10.1029/2010JD013943.

Fischer, E. V., D. A. Jaffe, D. R. Reidmiller, and L. Jaeglé (2010b), Meteorological controls on
observed peroxyacetyl nitrate at Mount Bachelor during the spring of 2008, *Journal of
Geophysical Research*, *115*, D03302, doi:10.1029/2009jd012776.

Flannigan, M. D., M. A. Krawchuk, W. J. de Groot, B. M. Wotton, and L. M. Gowman (2009),
Implications of changing climate for global wildland fire, *Int J Wildland Fire*, *18*(5), 483-507.

Forrister, H., J. Liu, E. Scheuer, J. Dibb, L. Ziemba, K. L. Thornhill, B. Anderson, G. Diskin, A.
E. Perring, and J. P. Schwarz (2015), Evolution of brown carbon in wildfire plumes, *Geophysical
Research Letters*, *42*(11), 4623-4630.

Gratz, L. E., D. A. Jaffe, and J. R. Hee (2014), Causes of increasing ozone and decreasing carbon
monoxide in springtime at the Mt. Bachelor Observatory from 2004 to 2013, *Atmospheric
Environment*, doi:10.1016/j.atmosenv.2014.05.076.

Hand, J. L., and W. C. Malm (2007), Review of aerosol mass scattering efficiencies from
ground-based measurements since 1990, *Journal of Geophysical Research*, *112*, D16203,
doi:10.1029/2007jd008484.

Haywood, J., and O. Boucher (2000), Estimates of the direct and indirect radiative forcing due to
tropospheric aerosols: A review, *Reviews of Geophysics*, *38*(4), 513-543,
doi:10.1029/1999rg000078.

Hinds, W. C. (1999), *Aerosol Technology: Properties, Behavior, and Measurement of Airborne
Particles, 2nd Edition*, John Wiley & Sons, Inc., New York.

Hobbs, P. V. (2003), Evolution of gases and particles from a savanna fire in South Africa,
Journal of Geophysical Research, *108*, doi:10.1029/2002jd002352.

Holder, A. L., G. S. Hagler, J. Aurell, M. D. Hays, and B. K. Gullett (2016), Particulate matter
and black carbon optical properties and emission factors from prescribed fires in the southeastern
United States, *J. Geophys. Res.*, *121*(7), 3465-3483.

Hosseini, S., Q. Li, D. Cocker, D. Weise, A. Miller, M. Shrivastava, J. W. Miller, S.
Mahalingam, M. Princevac, and H. Jung (2010), Particle size distributions from laboratory-scale
biomass fires using fast response instruments, *Atmospheric Chemistry and Physics*, *10*(16),
8065-8076, doi:10.5194/acp-10-8065-2010.

http://www-calipso.larc.nasa.gov/ (2016), NASA The Cloud-Aerosol Lidar and Infrared
Pathfinder Satellite Observation (CALIPSO), edited.

https://worldview.earthdata.nasa.gov/ (2016), NASA WorldView.

Jaffe, D. A., E. Prestbo, P. Swartzendruber, P. Weiss-Penzias, S. Kato, A. Takami, S.
Hatakeyama, and Y. Kajii (2005), Export of atmospheric mercury from Asia, *Atmospheric
Environment*, *39*(17), 3029-3038, doi:10.1016/j.atmosenv.2005.01.030.

Janhäll, S., M. O. Andreae, and U. Pöschl (2010), Biomass burning aerosol emissions from
vegetation fires: particle number and mass emission factors and size distributions, *Atmospheric
Chemistry and Physics*, *10*(3), 1427-1439.

Jolleys, M. D., et al. (2015), Properties and evolution of biomass burning organic aerosol from
465   Canadian boreal forest fires, *Atmospheric Chemistry and Physics*, *15*(6), 3077-3095,
       doi:10.5194/acp-15-3077-2015.

Justice, C. O., L. Giglio, S. Korontzi, J. Owens, J. T. Morisette, D. Roy, J. Descloitres, S.
       Alleaume, F. Petitcolin, and Y. Kaufman (2002), The MODIS fire products, *Remote Sensing of
       Environment*, *83*(1-2), 244-262, doi:10.1016/s0034-4257(02)00076-7.

470   Kirchstetter, T. W., T. Novakov, and P. V. Hobbs (2004), Evidence that the spectral dependence
       of light absorption by aerosols is affected by organic carbon, *Journal of Geophysical Research-
       Atmospheres*, *109*(D21), 12, doi:10.1029/2004jd004999.

Kondo, Y., et al. (2011), Emissions of black carbon, organic, and inorganic aerosols from
       biomass burning in North America and Asia in 2008, *Journal of Geophysical Research-
475   Atmospheres*, *116*, 25, doi:10.1029/2010jd015152.

Levin, E. J. T., et al. (2010), Biomass burning smoke aerosol properties measured during Fire
       Laboratory at Missoula Experiments (FLAME), *Journal of Geophysical Research-Atmospheres*,
       115, 15, doi:10.1029/2009jd013601.

Liu, S., et al. (2014a), Aerosol single scattering albedo dependence on biomass combustion
480   efficiency: Laboratory and field studies, *Geophysical Research Letters*, *41*(2), 742-748,
       doi:10.1002/2013gl058392.

Liu, Y., S. Goodrick, and W. Heilman (2014b), Wildland fire emissions, carbon, and climate:
       Wildfire-climate interactions, *Forest Ecology and Management*, *317*, 80-96,
       doi:10.1016/j.foreco.2013.02.020.

485   Lowenthal, D. H., and N. Kumar (2004), Variation of mass scattering efficiencies in IMPROVE,
       Journal of the Air & Waste Management Association, *54*(8), 926-934.

Malm, W. C., and J. L. Hand (2007), An examination of the physical and optical properties of
       aerosols collected in the IMPROVE program, *Atmospheric Environment*, *41*(16), 3407-3427.

May, A. A., T. Lee, G. R. McMeeking, S. Akagi, A. P. Sullivan, S. Urbanski, R. J. Yokelson,
490   and S. M. Kreidenweis (2015), Observations and analysis of organic aerosol evolution in some
       prescribed fire smoke plumes, *Atmospheric Chemistry and Physics*, *15*(11), 6323-6335,
       doi:10.5194/acp-15-6323-2015.

May, A. A., E. J. T. Levin, C. J. Hennigan, I. Riipinen, T. Lee, J. L. Collett, J. L. Jimenez, S. M.
       Kreidenweis, and A. L. Robinson (2013), Gas-particle partitioning of primary organic aerosol
495   emissions: 3. Biomass burning, *Journal of Geophysical Research-Atmospheres*, *118*(19), 11327-
       11338, doi:10.1002/jgrd.50828.

May, A. A., et al. (2014), Aerosol emissions from prescribed fires in the United States: A
       synthesis of laboratory and aircraft measurements, *Journal of Geophysical Research-
       Atmospheres*, *119*(20), 11826-11849, doi:10.1002/2014jd021848.

500   McMeeking, G. R., E. Fortner, T. B. Onasch, J. W. Taylor, M. Flynn, H. Coe, and S. M.
       Kreidenweis (2014), Impacts of nonrefractory material on light absorption by aerosols emitted
       from biomass burning, *Journal of Geophysical Research-Atmospheres*, *119*, 12272-12286,
       doi:10.1002/2014jd021750.

McMeeking, G. R., S. M. Kreidenweis, C. M. Carrico, T. Lee, J. L. Collett, and W. C. Malm
505 (2005), Observations of smoke-influenced aerosol during the Yosemite Aerosol Characterization
Study: Size distributions and chemical composition, *Journal of Geophysical Research-
Atmospheres*, *110*(D9).

Okoshi, R., A. Rasheed, G. C. Reddy, C. J. McCrowey, and D. B. Curtis (2014), Size and mass
distributions of ground-level sub-micrometer biomass burning aerosol from small wildfires,
510 *Atmospheric Environment*, *89*, 392-402, doi:10.1016/j.atmosenv.2014.01.024.

Omar, A. H., D. M. Winker, M. A. Vaughan, Y. Hu, C. R. Trepte, R. A. Ferrare, K.-P. Lee, C. A.
Hostetler, C. Kittaka, and R. R. Rogers (2009), The CALIPSO automated aerosol classification
and lidar ratio selection algorithm, *Journal of Atmospheric and Oceanic Technology*, *26*(10),
1994-2014.

515 Pierce, J. R., K. Chen, and P. J. Adams (2007), Contribution of primary carbonaceous aerosol to
cloud condensation nuclei: processes and uncertainties evaluated with a global aerosol
microphysics model, *Atmospheric Chemistry and Physics*, *7*(20), 5447-5466.

Pitchford, M., W. Malm, B. Schichtel, N. Kumar, D. Lowenthal, and J. Hand (2007), Revised
algorithm for estimating light extinction from IMPROVE particle speciation data, *Journal of the
520 Air & Waste Management Association*, *57*(11), 1326-1336.

Reid, J. S., T. F. Eck, S. A. Christopher, R. Koppmann, O. Dubovik, D. P. Eleuterio, B. N.
Holben, E. A. Reid, and J. Zhang (2005a), A review of biomass burning emissions part III:
intensive optical properties of biomass burning particles, *Atmospheric Chemistry and Physics*, *5*,
827-849.

525 Reid, J. S., R. Koppmann, T. F. Eck, and D. P. Eleuterio (2005b), A review of biomass burning
emissions part II: intensive physical properties of biomass burning particles, *Atmospheric
Chemistry and Physics*, *5*, 799-825, doi:10.5194/acp-5-799-2005.

Reidmiller, D. R., D. A. Jaffe, E. V. Fischer, and B. Finley (2010), Nitrogen oxides in the
boundary layer and free troposphere at the Mt. Bachelor Observatory, *Atmospheric Chemistry
530 and Physics*, *10*(13), 6043-6062, doi:10.5194/acp-10-6043-2010.

Sakamoto, K., J. Allan, H. Coe, J. Taylor, T. Duck, and J. Pierce (2015), Aged boreal biomass-
burning aerosol size distributions from BORTAS 2011, *Atmospheric Chemistry and Physics*,
15(4), 1633-1646.

Sakamoto, K., R. Stevens, and J. Pierce (In Press), The evolution of biomass-burning aerosol
535 size distributions due to coagulation: dependence on fire and meteorological details and
parameterization, *Atmospheric Chemistry and Physics*.

Seinfeld, J. H., and S. N. Pandis (2006), *Atmospheric Chemistry and Physics: From Air
Pollution to Climate Change 2nd Edition*, John Wiley & Sons, Inc., Hoboken, New Jersey.

Spracklen, D. V., K. S. Carslaw, U. Poschl, A. Rap, and P. M. Forster (2011), Global cloud
540 condensation nuclei influenced by carbonaceous combustion aerosol, *Atmospheric Chemistry
and Physics*, *11*(17), 9067-9087, doi:10.5194/acp-11-9067-2011.

Stein, A. F., R. R. Draxler, G. D. Rolph, B. J. B. Stunder, M. D. Cohen, and F. Ngan (2015),
NOAA'S HYSPLIT ATMOSPHERIC TRANSPORT AND DISPERSION MODELING

SYSTEM, *Bulletin of the American Meteorological Society*, *96*(12), 2059-2077,
545   doi:10.1175/bams-d-14-00110.1.

Stocks, B. J., et al. (1998), Climate change and forest fire potential in Russian and Canadian
boreal forests, *Climatic Change*, *38*(1), 1-13, doi:10.1023/a:1005306001055.

Timonen, H., D. A. Jaffe, N. Wigder, J. Hee, H. Gao, L. Pitzman, and R. A. Cary (2014),
Sources of carbonaceous aerosol in the free troposphere, *Atmospheric Environment*, *92*(0), 146-
550   153, doi:http://dx.doi.org/10.1016/j.atmosenv.2014.04.014.

Timonen, H., N. Wigder, and D. Jaffe (2013), Influence of background particulate matter (PM)
on urban air quality in the Pacific Northwest, *Journal of Environmental Management*, *129*, 333-
340, doi:10.1016/j.jenvman.2013.07.023.

Vakkari, V., et al. (2014), Rapid changes in biomass burning aerosols by atmospheric oxidation,
555   *Geophysical Research Letters*, *41*(7), 2644-2651, doi:10.1002/2014gl059396.

Virkkula, A. (2010), Correction of the Calibration of the 3-wavelength Particle Soot Absorption
Photometer (3 PSAP), *Aerosol Science and Technology*, *44*(8), 706-712,
doi:10.1080/02786826.2010.482110.

Weiss-Penzias, P., D. Jaffe, P. Swartzendruber, W. Hafner, D. Chand, and E. Prestbo (2007),
560   Quantifying Asian and biomass burning sources of mercury using the Hg/CO ratio in pollution
plumes observed at the Mount Bachelor Observatory, *Atmospheric Environment*, *41*(21), 4366-
4379, doi:10.1016/j.atmosenv.2007.01.058.

Weiss-Penzias, P., D. A. Jaffe, P. Swartzendruber, J. B. Dennison, D. Chand, W. Hafner, and E.
Prestbo (2006), Observations of Asian air pollution in the free troposphere at Mount Bachelor
565   Observatory during the spring of 2004, *Journal of Geophysical Research-Atmospheres*,
111(D10), D10304-D10304, doi:10.1029/2005JD006522.

Westerling, A. L., H. G. Hidalgo, D. R. Cayan, and T. W. Swetnam (2006), Warming and earlier
Spring increase western U.S. forest wildfire activity, *Science*, *313*, 940-943.

Wiedinmyer, C., S. K. Akagi, R. J. Yokelson, L. K. Emmons, J. A. Al-Saadi, J. J. Orlando, and
570   A. J. Soja (2011), The Fire INventory from NCAR (FINN): a high resolution global model to
estimate the emissions from open burning, *Geoscience Model Development*, *4*, 625-641,
doi:10.5194/gmd-4-625-2011.

Wigder, N. L., D. A. Jaffe, and F. A. Saketa (2013), Ozone and particulate matter enhancements
from regional wildfires observed at Mount Bachelor during 2004-2011, *Atmospheric
575   Environment*, *75*, 24-31, doi:10.1016/j.atmosenv.2013.04.026.

Winker, D. M., J. Pelon, J. Coakley Jr, S. Ackerman, R. Charlson, P. Colarco, P. Flamant, Q. Fu,
R. Hoff, and C. Kittaka (2010), The CALIPSO mission: A global 3D view of aerosols and
clouds, *Bulletin of the American Meteorological Society*, *91*(9), 1211.

Winker, D. M., M. A. Vaughan, A. Omar, Y. Hu, K. A. Powell, Z. Liu, W. H. Hunt, and S. A.
580   Young (2009), Overview of the CALIPSO mission and CALIOP data processing algorithms,
Journal of Atmospheric and Oceanic Technology, *26*(11), 2310-2323.

Yokelson, R. J., M. O. Andreae, and S. K. Akagi (2013a), Pitfalls with the use of enhancement
ratios or normalized excess mixing ratios measured in plumes to characterize pollution sources

and aging, *Atmospheric Measurement Techniques*, *6*, 2155-2158, doi:10.5194/amtd-6-4077-
585   2013.

Yokelson, R. J., et al. (2013b), Coupling field and laboratory measurements to estimate the
emission factors of identified and unidentified trace gases for prescribed fires, *Atmospheric
Chemistry and Physics*, *13*(1), 89-116, doi:10.5194/acp-13-89-2013.

Yokelson, R. J., et al. (2009), Emissions from biomass burning in the Yucatan, *Atmospheric
590   Chemistry and Physics*, *9*, 5785-5812, doi:10.5194/acp-9-5785-2009.

Table 1. Identified BB plumes at MBO during the summer of 2015. All enhancement ratios are obtained by taking the slope of a RMA linear regression between the two species. ND ("no data") indicates missing data. WC in the MAE column signifies a weak correlation ($R^2 < 0.60$).

Event number	Event date and time (UTC)	Event duration (hours)	Source fire location	ΔWV (g/kg)	$\Delta\sigma_{scat}/\Delta CO$ (Mm^{-1}/ppbv)	$\Delta\sigma_{abs}/\Delta CO$ (Mm^{-1}/ppbv)	MSE (m^2/g)	MAE (m^2/g)	AAE (467-660 nm)	ω (528 nm)	D_{pm} (nm)	σ_g
1	7/31/15 15:35-17:10	1.58	OR	0.16	1.13	0.036	ND	ND	3.15	0.97	164	1.72
2	8/9/15 2:55-8:55	6.00	CA, OR	1.62	0.89	WC	3.17	0.085	3.45	0.98	138	1.82
3	8/9/15 13:35-8/10/15 0:00	10.42	CA, OR	2.07	1.24	0.033	3.29	0.087	3.72	0.98	156	1.70
4	8/10/15 1:10-5:55	4.75	CA, OR	1.86	1.05	0.030	3.78	0.108	3.86	0.97	182	1.54
5	8/10/15 6:05-11:40	5.58	CA, OR	1.25	1.09	0.034	3.44	0.106	4.02	0.97	183	1.61
6	8/10/15 11:45-14:35	2.83	CA, OR	1.32	0.94	WC	3.27	WC	4.12	0.99	177	1.61
7	8/10/15 14:40- 8/11/15 6:15	15.58	CA, OR	1.83	1.17	0.032	3.64	0.098	3.52	0.98	186	1.62
8	8/11/15 14:20-18:45	4.42	CA, OR	1.11	1.07	0.029	2.50	0.066	2.74	0.98	160	1.78
9	8/14/15 10:00-15:35	5.58	OR	1.12	0.48	0.007	2.75	0.042	3.06	0.99	165	1.67
10	8/17/15 0:05-3:55	3.83	Siberian	-0.87	1.39	0.078	ND	ND	2.48	0.95	176	1.57
11	8/17/15 17:15- 8/18/15 7:00	13.75	Siberian	-0.22	1.06	0.060	ND	ND	2.50	0.95	179	1.69
12	8/18/15 16:05 - 8/19/15 16:40	24.58	Siberian	0.56	1.29	0.075	ND	ND	2.30	0.95	196	1.64
13	8/19/15 17:40 - 8/20/15 3:05	9.42	Siberian	0.60	1.12	0.052	ND	ND	2.25	0.96	175	1.76
14	8/22/15 15:30-18:05	2.58	Siberian	-3.10	1.97	0.078	4.76	0.188	3.59	0.96	229	1.73
15	8/23/15 3:55-7:00	3.08	Siberian	-2.45	1.09	0.059	2.84	0.156	2.51	0.96	162	1.89
16	8/23/15 9:50- 8/25/15 6:50	45.00	CA, OR	1.00	1.13	0.029	4.06	0.107	3.15	0.98	205	1.58
17	8/25/15 12:45 - 8/26/15 19:00	30.25	CA, OR	1.67	0.88	0.027	3.75	0.111	3.12	0.98	181	1.60
18	8/26/15 7:15 - 8/28/15 11:15	40.00	CA, OR	1.35	0.89	0.031	3.70	0.128	3.48	0.97	191	1.53
19	8/28/15 17:40 - 8/29/15 6:15	12.58	CA, OR	1.54	0.69	ND	2.94	ND	ND	ND	164	1.58

ΔWV is water vapor enhancement, calculated for each event by subtracting the average WV for the summer sampling period from the WV value at the time when maximum CO was observed.

Aerosol scattering σ_{scat} (550 nm) and absorption σ_{abs} (528 nm) measurements were converted to STP.

MSE and MAE calculated as the $\Delta\sigma_{scat}/\Delta PM1$ and $\Delta\sigma_{abs}/\Delta PM1$ enhancement ratios, respectively.

D_{pm} is the geometric mean diameter and σ_g is the geometric standard deviation of the SMPS aerosol size distribution.

WC indicates a weak correlation in the MAE column ($R^2 < 0.60$).

ND indicates missing data. PM data was not available for events 1 and 10-13; absorption data was not available for events 19 and 20.

Figures:
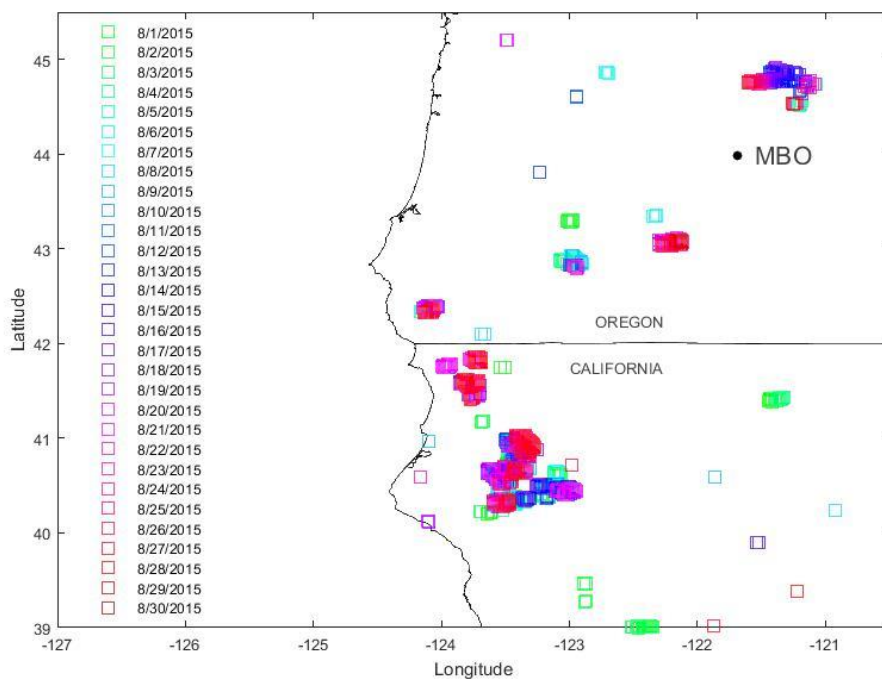
Figure 1. MBO and MODIS firespots colored by date for the month of August.
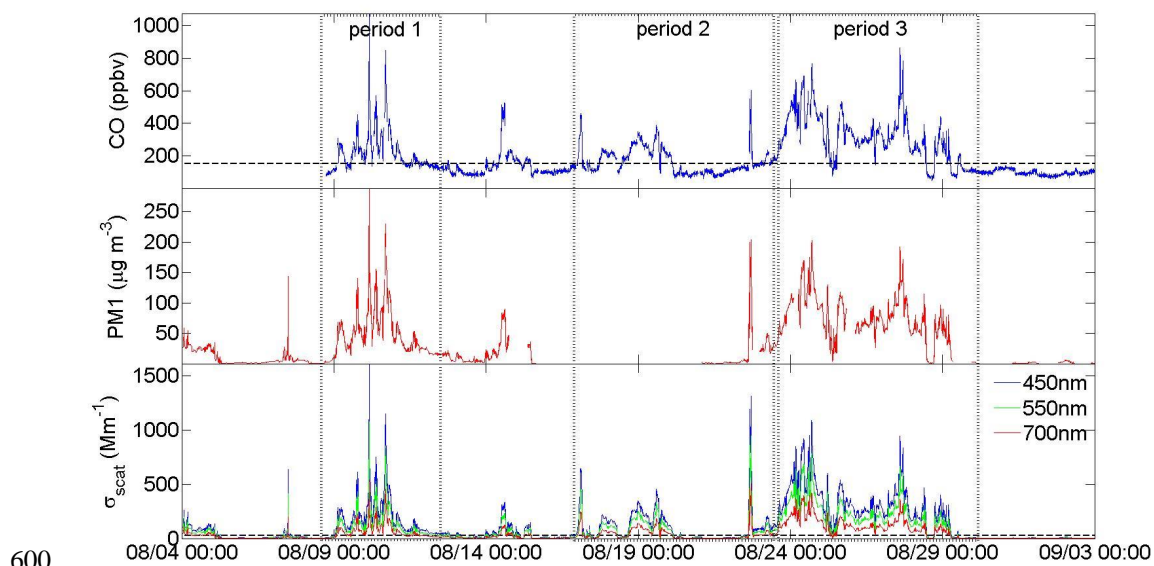
600

Figure 2. Time series of (i) CO, (ii) PM1, and aerosol scattering (σ$_{scat}$) (iii) at MBO during August. Threshold values (dashed black lines) used for BB event criteria are displayed for CO (150 ppbv) and scattering (20 Mm^{-1}). Three period are identified by dotted boxes. Periods 1 and 3 are regionally influenced and encompass events 2-8 and 16-19, respectively. Period 2 is

605   influenced by Siberian BB and encompasses events 10-15.
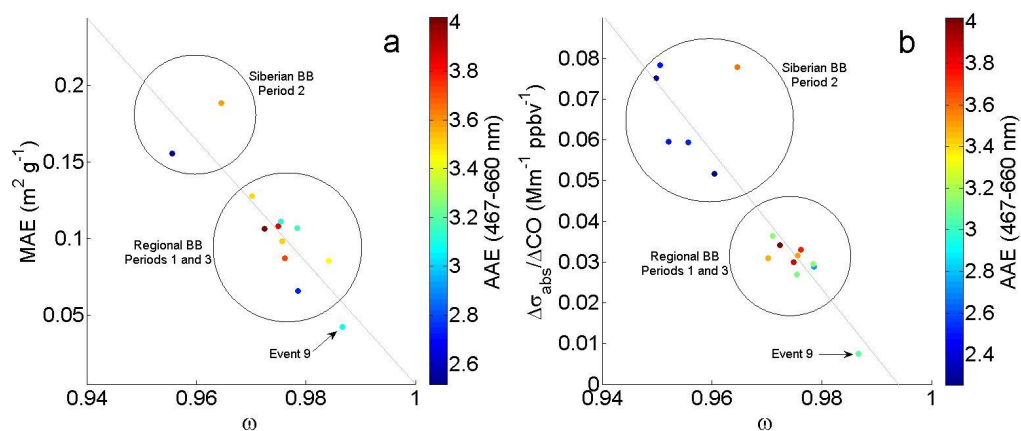
Figure 3. Scatter plots of (a) mass absorption efficiency (MAE) (b) absorption enhancement ratio $\Delta\sigma_{abs}/\Delta CO$ versus single scattering albedo (ω). MAE values were not calculated for four of
610   the six Siberian influenced events due to missing PM1 data.
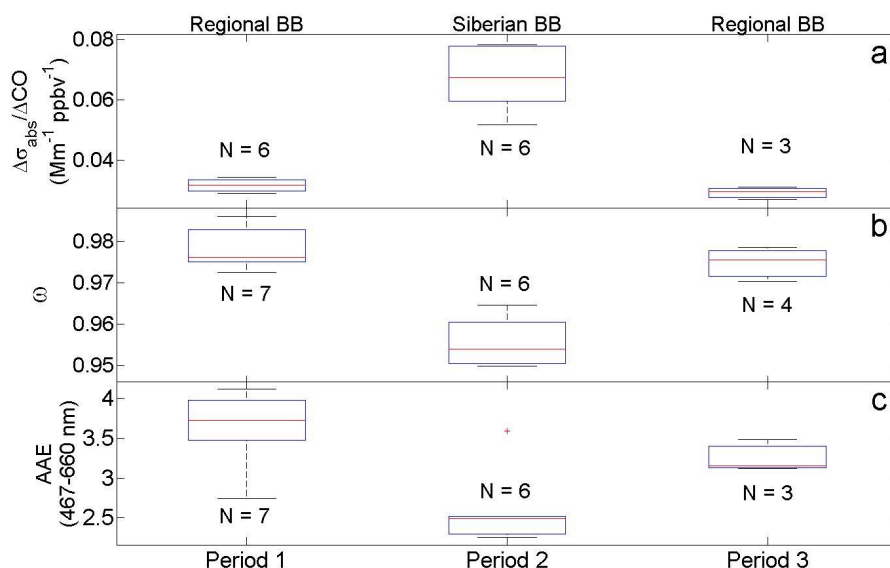
Figure 4. Boxplots of (a) $\Delta\sigma_{abs}/\Delta CO$, (b) single scattering albedo (ω) measured at 528 nm, and (c) absorption Ångström exponent (AAE) for absorption measurements at 467 and 660 nm for the three periods shown in Figure 2. Periods 1 and 3 represent regional BB events, and period 2 consists of Siberian influenced events. N indicates the number of events for each box. Lower and upper whiskers represent the minimum and maximum values, respectively. Lower and upper lines of the box represent the 25th and 75th percentiles, respectively. The red line at the middle of the box represents the median, and the red plus mark represents outliers.
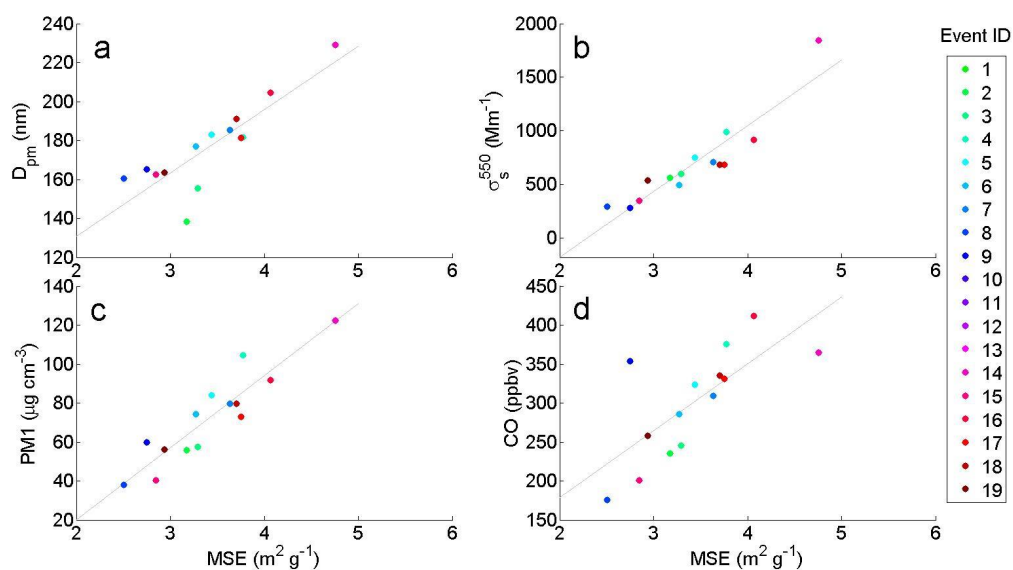
625   **Figure 5.** Scatter plots of (a) D_{pm} ($R^2 = 0.73$), (b) σ_{scat} ($R^2 = 0.90$), (c) PM1 ($R^2 = 0.85$), and (d) CO ($R^2 = 0.53$) versus mass scattering efficiency (MSE) for the BB events at MBO in the summer of 2015.
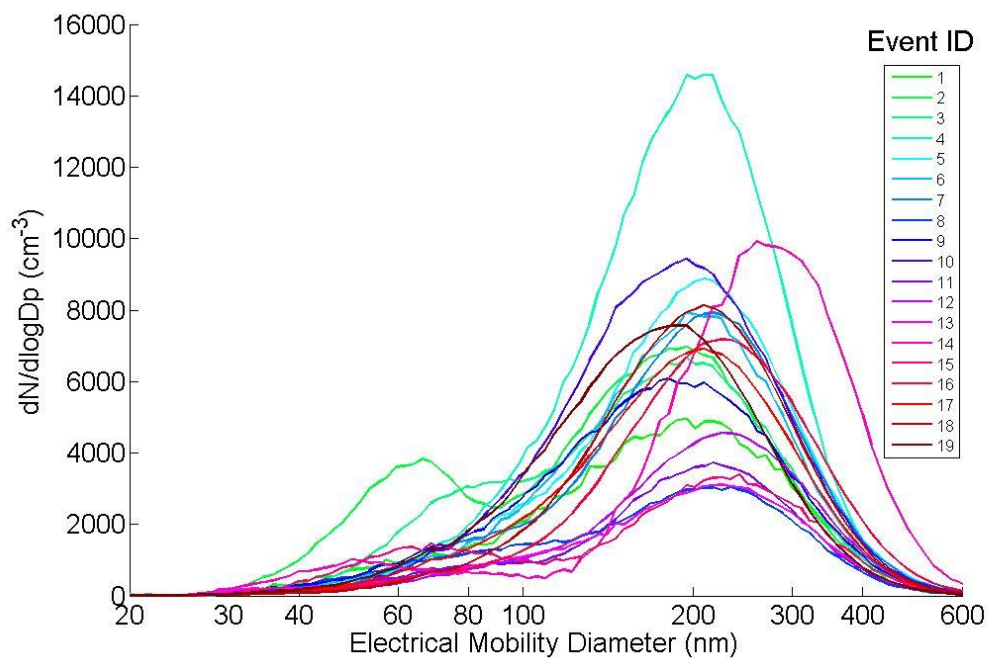
630

Figure 6. Event integrated aerosol number size distributions (corrected to STP) in dN/dlogDp (# cm⁻¹).